Supporting Information

Shiraiwa et al. 10.1073/pnas.1103045108

SI Text

Estimation of Diffusion Coefficients. ***Estimation of D_{org}.*** In order to estimate the self-diffusion coefficient of bovine serum albumin (BSA) in BSA/water mixtures we used data of the viscosity of aqueous BSA solutions by Brownsey et al. (1) shown as red circles in Fig. S3. The data cover a range of dilute to concentrated solutions up to a BSA mass fraction of 0.5. Moreover, Brownsey et al (1) and Hottot et al (2) suggested that at room temperature aqueous BSA turns into a glass at a mass fraction between 0.6–0.8. Therefore, we chose a representative value of the viscosity at T_g of 10^{12} Pa s at a BSA mass fraction of 0.7, see blue square in Fig. S3. Using these data we can fit the viscosity (ν) of aqueous BSA over the whole concentration range, which can be estimated as follows:

$$\ln(\nu) = \ln(\nu_0) + \frac{\ln(\nu_{max})}{1+\exp(\frac{w_c - w}{s})} + Aw(1-\tanh(w-w_c)), \quad \textbf{[S1]}$$

where ν_0 is the viscosity of water (8.9×10^{-4} Pa s), ν_{max} is the characteristic viscosity in the glass transition ($\sim 10^{12}$–10^{13} Pa s, here: 7.53×10^{12} Pa s), w is the BSA mass fraction, $w_c = 0.514$ is the critical BSA mass fraction at which the BSA globules begin to come into contact with each other, $s = 0.041, A = 9.32$ is a constant characteristic of the near linear increase in $\ln(\nu)$ at small BSA mass fractions, and the term $1 - \tanh(w\text{-}w_c)$ is responsible for saturating this increase to a constant at concentration higher than about w_c.

The function in Eq. **S1** was chosen such that once the translational motion of globular BSA proteins seizes close to T_g, the viscosity remains practically constant at a value of about that at T_g (red dashed line), which is however, not relevant for the investigated concentration range investigated in Mikhailov et al. (3) and this work. Note that the steepest change in viscosity occurs around a mass fraction of 0.5–0.6, in agreement with experimental observations of Brownsey et al. (1), who observed a "glass-like kinetic arrest" at mass fractions in the region of 0.55.

The green triangles shown in Fig. S3 are inferred from the hygroscopicity tandem differential mobility analyzer (HTDMA) experiments by Mikhailov et al. (3). From these data, the water content of BSA aerosol particles as a function of relative humidity was calculated assuming a void fraction of 0.3, in agreement with a glass-transition induced fixation of BSA globules at a mass fraction of ~0.7, which is close to a dense packing of spheres. Fig. S3 implies that the BSA particles experience the entire semisolid range upon changes in humidity, with near-liquid viscosity/diffusivity at RH $\geq$ ~95% and near-solid behavior at RH $\leq$ ~30%.

The resulting viscosity values of aqueous BSA range from ν of 10^1–10^{12} Pa s depending on relative humidity. Using Eq. 1 in the main text, this viscosity can be converted to D_{org} values assuming a radius for globular BSA of $a = 2.5$ nm. As RH increased, D_{org} increases as particles take up more water.

Estimation of D_{ox}. The diffusion coefficient of ozone in the aqueous BSA film is estimated using the percolation theory (4–6), because the Stokes-Einstein equation is not applicable for small gas molecules diffusing through a highly viscous heterogeneous matrix near the glass-transition temperature (7). According to percolation and effective medium theory, the average diffusion coefficient in a mixture of two media with different diffusion can be described by the following equation:

$$D_{ox} = [D'_{ox,p} + D'_{ox,w} + [(D'_{ox,p} + D'_{ox,w})^2 + 2(Z-2)D_{ox,p}D_{ox,w}]]/(Z-2), \quad \textbf{[S2]}$$

where $D_{ox,p}$ is the diffusion coefficient of oxidant in protein globules, and $D_{ox,w}$ is the diffusion coefficient of oxidant in water ($\sim 10^{-5}$ cm^2 s^{-1}), which can be calculated by $D_{O_3,w}$ (cm^{2}s^{-1}) = $1.1 \times 10^{-4} \exp(-1{,}896/T)$ (8). $D'_{ox,p}$ and $D'_{ox,w}$ are reduced diffusion coefficients and are expressed as:

$$D'_{ox,p} = [(Z/2)(V_p/f) - 1]D_{ox,p} \quad \textbf{[S3]}$$

$$D'_{ox,w} = [(Z/2)(1 - V_p/f) - 1]D_{ox,w}. \quad \textbf{[S4]}$$

V_p is the volume fraction of protein globules, which can be directly calculated using hygroscopic growth factor (GF) data measured for BSA (3): $V_p = (1/GF)^3$. f is the packing fraction, for which we assumed a value of 0.85 (9). Z is the coordination number between water-filled pores in the protein matrix, for which we assumed a value of 12 that is characteristic for dense sphere packings (10). For $D_{ox,p}$ we assumed a value of 5×10^{-10} cm^2 s^{-1} which is of a magnitude characteristic for diffusion of small molecules solids (Table 1) and consistent with the diffusion-limited uptake of ozone observed under dry conditions (Fig. 2). For uncertainty estimates (green shaded area), f was varied from 0.65 to 1 (4, 9, 11), Z was varied between 8 and 16 (4), and $D_{ox,p}$ was varied from 10^{-10}–10^{-9} cm^2 s^{-1} (12).

The temperature dependence of D_{ox} at 50% RH was estimated using an Arrhenius-approach with an activation energy of about 15.8 kJ mol^{-1} (8) (Fig. S4).

Ozone Uptake Experiments. Fig. S5 shows the ozone uptake observed with an initial gas phase O_3 concentration of ~110 ppb at 50% RH. At the beginning of each experiment, the coated wall flow tube was bypassed to obtain a stable ozone signal ($t < 0$). When the flow was redirected through the flow tube ($t = 0$), the gas phase O_3 concentration dropped rapidly to ~60 ppb, which corresponds to an ozone uptake coefficient of $\gamma_{O_3} \approx 10^{-5}$ during the first few seconds of reaction time ($t \approx 10$ s). Then the ozone concentration recovered asymptotically towards the initial value, and the uptake coefficient exhibited a strong decrease that continued over multiple hours (Fig. 3). When the flow tube was bypassed again (e.g., at $t \approx 3{,}000$ s in Fig. S5), the gas phase ozone concentration quickly returned to the initial value, showing that the experimental conditions were stable. No significant ozone uptake was observed in an uncoated glass flow tube, confirming that the observed ozone loss was due to uptake by the protein film on the wall of the coated tube.

The magnitude and temporal evolution of γ_{O_3} did not change when the thickness of the protein film on the flow tube walls was varied between 133–346 nm. This finding indicates that the ozone uptake was kinetically limited by processes at or near the surface of the protein film. If the uptake kinetics had been affected by processes involving the entire volume of the protein film, the film thickness should have influenced the results, i.e., thicker films should have exhibited higher values or slower decrease of γ_{O_3}. Moreover, the amount of ozone taken up by the protein film ($>1 \times 10^{14}$ cm^{-2} after 1 h) clearly exceeded the surface capacity of reaction sites ($\lesssim 3 \times 10^{13}$ cm^{-2}). Thus, the most plausible explanation for the observed behavior is that the uptake of ozone was limited by diffusion and reaction near the surface of the protein film.

Kinetic Models and Parameters. Two kinetic flux models were applied to analyze the experimental results: the kinetic multilayer model (KM-SUB) (13) and the kinetic double-layer model (K2-SUB) (14) for aerosol surface and bulk chemistry, both of which build on the formalism and terminology of the PRA framework (15, 16). The uptake coefficient of ozone (γ_{O_3}) is defined as the ratio between the net flux of O_3 from the gas phase to the condensed phase and the gas kinetic flux of O_3 colliding with the surface (13, 14). The temporal evolution of γ_{O_3} and the particle surface and bulk composition were modeled by numerically solving the differential equations for the mass balance of each model compartment with Matlab (ode23tb solver with 999 time steps).

KM-SUB consists of multiple model compartments and layers: gas phase, near-surface gas phase, sorption layer, quasi-static surface layer, near-surface bulk, and a number of bulk layers as detailed below. KM-SUB explicitly treats all steps of mass transport (gas phase diffusion, gas-surface transport, and bulk diffusion) and chemical reactions from the gas-particle interface to the particle core, resolving concentration gradients and diffusion throughout the particle bulk. Unlike traditional resistor models, KM-SUB does not require simplifying assumptions about steady-state conditions and radial mixing. Surface-bulk transport and bulk diffusion of volatile and nonvolatile reactants are treated as the mass transport from one bulk layer to the next by describing the mass transport fluxes between different layers of the bulk by first-order transport velocities, which are calculated from the bulk diffusion coefficients (13). Bulk reaction rates are calculated assuming that bulk reactions proceed with second-order rate dependencies on the concentrations within each bulk layer. In the numerical simulations presented in this study, the number of model layers was set to $n = 200$ unless mentioned otherwise. Test calculations using smaller or higher values of n gave very similar results. The maximum relative deviations were 10% for $n < 20$, reconfirming the robustness of the KM-SUB model approach (13).

Instead of explicitly resolving radial profiles of bulk diffusion and reaction, K2-SUB (14) uses just one layer for the bulk, and the effects of bulk diffusion and reaction are represented by the reacto-diffusive flux ($J_{b,rd}$) based on traditional resistor model formulations (15,17–19). In this approach, the nonvolatile reactant is assumed to be well mixed in the bulk of the condensed phase (14). While the original K2-SUB model presented by Pfrang et al. (2009) (14) also assumed steady-state conditions for O_3 on the surface and in the bulk, we used the modified K2-SUB model of Shiraiwa et al. (2010) (13) without these steady-state assumptions (13).

The initial concentrations of ozone at the surface and in the bulk were set to zero, and the kinetic input parameters are listed in Table S1: surface accommodation coefficient of ozone for the clean substrate ($\alpha_{s,0}$), desorption lifetime of ozone (τ_d), bulk diffusion coefficients of ozone and reactive amino acids (D_{ox}, D_{org}), and second-order rate coefficients for the reaction between ozone and amino acids at the surface and in the bulk (k_{SLR} and k_{BR}), and the Henry's law coefficient of ozone ($K_{sol,cc}$). Additional input parameters are the mean thermal velocity of ozone ($\omega = 3.6 \times 10^4$ cm s^{-1}) and the effective molecular diameter of ozone ($\delta_{O_3} = 0.4$ nm) (14).

Among the 20 standard amino acids occurring in proteins, five are known to react with ozone: cysteine [35], methionine [5], tryptophan [3], tyrosine [21], and histidine [16] (20–22); the number in brackets shows the number of amino acid residues in one BSA molecule. The second-order rate coefficients of the reaction between these reactive amino acids and ozone in water at around pH7 vary by about three orders of magnitude from 10^5–10^7 M^{-1} s^{-1} (20, 23). For simplicity, we assume that ozone reacts with these amino acids with the same reactivity of 10^6 M^{-1} s^{-1} (1.6×10^{-15} cm^3 s^{-1}). Considering the BSA molecular mass (67 kDa) and density (1.36 g cm^{-3}) and assuming that the BSA protein molecules are densely packed, the BSA concentration is calculated to be 4.5×10^{18} cm^{-3}. Here we assume that one quarter of the reactive amino acids in the protein can be reacted (24, 25), resulting in the initial surface and bulk concentrations of these reactive amino acids of 3.3×10^{13} cm^{-2} and 9.0×10^{19} cm^{-3}, respectively.

Initial estimates for the required kinetic parameters are based on our previous studies (13, 14, 16, 26) and typical ranges for the interactions between ozone and organic surfaces: $\alpha_{s,0} = 10^{-3} - 1$, $\tau_d = 10^{-10} - 1$, $k_{SLR} = 10^{-18} - 10^{-11}$ cm^2 s^{-1}, and $K_{sol,cc} = 10^{-5}$–10^{-3} mol cm^{-3} atm^{-1}. These parameters were systematically and iteratively varied using Matlab software to find a best fit solution as summarized in Table S1. As specified below, the optimized parameter combination given in Table S1 is not a unique solution and other parameter combinations can also match the observed uptake coefficients. However, the key results presented in our study remain unchanged. In particular, the range of available literature data on the reaction rate coefficients and Henry's law coefficients of ozone in organic matrices does limit the range of diffusion coefficients that we extracted by applying KM-SUB to the experimental data observed as a function of time, O_3, and RH. The corresponding ranges of uncertainty are indicated by the error bars in Fig. 2.

Sensitivity Studies. In order to characterize the sensitivity of the model results with regard to the chosen set of kinetic input parameters, all parameters in Table S1 were varied systematically. The sensitivity studies revealed that $\alpha_{s,0}$, τ_d, and k_{SLR} are not critical for describing the observations of γ_{O_3} over the time scales of the experiments performed (>10 s); much higher time resolution would be required to resolve the surface processes. Even if the surface reaction is switched off (i.e., $k_{SLR,X,Y} = 0$), the model can reproduce the observed γ_{O_3} because uptake kinetics was limited by surface-bulk transport and bulk diffusion of ozone. The uptake of O_3 is insensitive to k_{BR} as long as it exceeds 10^{-16} cm^2 s^{-1}, indicating that for the reaction of ozone with amino acids under our experimental conditions, uptake was not kinetically limited by bulk reaction. If both the surface and bulk reactions are switched off, the calculated ozone concentration profiles (Fig. S6) reflects a nonreactive saturation process with a characteristic diffusion time as discussed in the main text (Fig. 1 and Eq. 1).

The most sensitive parameter is found to be D_{ox}, confirming that bulk diffusion of ozone is the rate-limiting step. The sensitivity study suggests that D_{ox} should be in the range of 5×10^{-10} – 10^{-8} cm^2 s^{-1} at 50% RH, which is consistent with predictions of Fig. 2*B*. D_{ox}, $K_{sol,cc}$, and k_{BR} can be mutually adjusted to match the observed γ_{O_3}; for example, the data can be also reproduced with $D_{ox} = 10^{-8}$ cm^2 s^{-1}, $K_{sol,cc} = 10^{-4}$ mol cm^{-3} atm^{-1}, and $k_{BR} = 1.6 \times 10^{-14}$ cm^3 s^{-1}. The reported k_{BR} (10^{-17}–10^{-14} cm^3 s^{-1}) and $K_{sol,cc}$ ($\sim 10^{-4}$ mol cm^{-3} atm^{-1}) limit the range of D_{ox} to match the kinetic observations and modeling.

The sensitivity study suggests that D_{org} should be below 10^{-17} cm^2 s^{-1} at 50% RH in order to be consistent with the experimental data. For values smaller than 10^{-17} cm^2 s^{-1}, the actual value becomes unimportant. This result implies that a potential breakdown of the Stokes-Einstein near the glass-transition is not relevant for the self-diffusion coefficient D_{org}. If a larger value for D_{org} is used, the second plateau of γ_{O_3} extends, showing similar behavior as K2-SUB in Fig. 5*A*. In this case Org is transported to the near-surface bulk to react with ozone there, so that diffusion of ozone is not the limiting step any more.

1. Brownsey GJ, Noel TR, Parker R, Ring SG (2003) The glass-transition behavior of the globular protein bovine serum albumin. *Biophys J* 85:3943–3950.

2. Hottot A, Daoussi R, Andrieu J (2006) Thermophysical properties of aqueous and frozen states of BSA/water/Tris systems. *Int J Biol Macromol* 38:225–231.

3. Mikhailov E, Vlasenko S, Niessner R, Pöschl U (2004) Interaction of aerosol particles composed of protein and salts with water vapor: hygroscopic growth and microstructural rearrangement. *Atmos Chem Phys* 4:323–350.
4. Murata T, Lee MS, Tanioka A (1999) An application of percolation theory to the electrolyte penetration through porous water-swollen cellulose triacetate membrane. *J Colloid Interface Sci* 220:250–254.
5. Shante VKS, Kirkpatrick S (1971) Introduction to percolation theory. *Adv Phys* 20:325–357.
6. Sherman RD, Middleman LM, Jacobs SM (1983) Electron-transport processes in conductior-filled polymers. *Polym Eng Sci* 23:36–46.
7. Champion D, Le Meste M, Simatos D (2000) Towards an improved understanding of glass-transition and relaxations in foods: molecular mobility in the glass-transition range. *Trends Food Sci Technol* 11:41–55.
8. Johnson PN, Davis RA (1996) Diffusivity of ozone in water. *J Chem Eng Data* 41:1485–1487.
9. Farr RS, Groot RD (2009) Close packing density of polydisperse hard spheres. *J Chem Phys* 131:244104.
10. Kittel C (1996) *Introduction to Solid State Physics* (Wiley, New York).
11. Fitzpatrick J, Malt RB, Spaepen F (1974) Percolation theory and conductivity of random close packed mixtures of hard spheres. *Phys Lett A* 47:207–208.
12. Huthwelker T, Ammann M, Peter T (2006) The uptake of acidic gases on ice. *Chem Rev* 106:1375–1444.
13. Shiraiwa M, Pfrang C, Pöschl U (2010) Kinetic multilayer model of aerosol surface and bulk chemistry (KM-SUB): the influence of interfacial transport and bulk diffusion on the oxidation of oleic acid by ozone. *Atmos Chem Phys* 10:3673–3691.
14. Pfrang C, Shiraiwa M, Pöschl U (2010) Coupling aerosol surface and bulk chemistry with a kinetic double-layer model (K2-SUB): an exemplary study of the oxidation of oleic acid by ozone. *Atmos Chem Phys* 10:4357–4557.
15. Pöschl U, Rudich Y, Ammann M (2007) Kinetic model framework for aerosol and cloud surface chemistry and gas-particle interactions—Part 1: general equations, parameters, and terminology. *Atmos Chem Phys* 7:5989–6023.
16. Ammann M, Pöschl U (2007) Kinetic model framework for aerosol and cloud surface chemistry and gas-particle interactions—Part 2: exemplary practical applications and numerical simulations. *Atmos Chem Phys* 7:6025–6045.
17. Danckwerts PV (1951) Absorption by simultaneous diffusion and chemical reaction into particles of various shapes and into falling drops. *Trans Faraday Soc* 47:1014–1023.
18. Hanson DR (1997) Surface-specific reactions on liquids. *J Phys Chem B* 101:4998–5001.
19. Worsnop DR, Morris JW, Shi Q, Davidovits P, Kolb CE (2002) A chemical kinetic model for reactive transformations of aerosol particles. *Geophys Res Lett* 29:57-1–57-4.
20. Sharma VK, Graham NJD (2010) Oxidation of amino acids, peptides and proteins by ozone: a review. *Ozone Sci Eng* 32:81–90.
21. Mudd JB, Leavitt R, Ongun A, McManus TT (1969) Reaction of ozone with amino acids and proteins. *Atmos Environ* 3:669–681.
22. Pryor WA, Giamalva DH, Church DF (1984) Kinetics of ozonation. 2. Amino acids and model compounds in water and comparisons to rates in nonpolar solvents. *J Am Chem Soc* 106:7094–7100.
23. Ignatenko AV, Cherenkevich SN (1985) Reactivity of amino-acids and proteins in reactions with ozone. *Kinet Catal* 26:1145–1148.
24. Zhang Y, Yang H, Pöschl U (2011) Analysis of nitrated proteins and tryptic peptides by HPLC-chip-MS/MS: site-specific quantification, nitration degree, and reactivity of tyrosine residues. *Anal Bioanal Chem* 399:459–471.
25. Yang H, Zhang Y, Pöschl U (2010) Quantification of nitrotyrosine in nitrated proteins. *Anal Bioanal Chem* 397:879–886.
26. Shiraiwa M, Garland RM, Pöschl U (2009) Kinetic double-layer model of aerosol surface chemistry and gas-particle interactions (K2-SURF): degradation of polycyclic aromatic hydrocarbons exposed to O_3, NO_2, H_2O, OH and NO_3. *Atmos Chem Phys* 9:9571–9586.

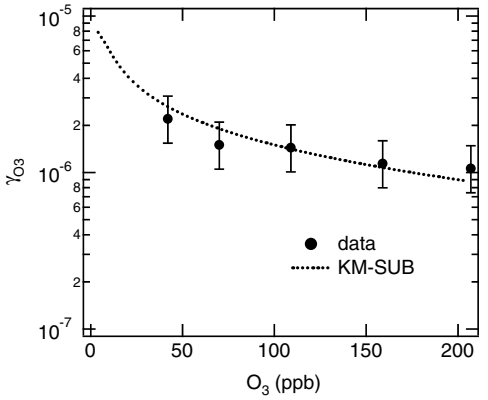

Fig. S1. Ozone uptake coefficients (γ_{O_3}) on BSA films (246 nm) at 50% RH as a function of gas phase ozone concentration after a reaction time of $t = 10^3$ s. The data points and error bars represent experimental data and standard deviations. The dotted line was calculated with the kinetic multilayer model KM-SUB using input parameters from Table S1.

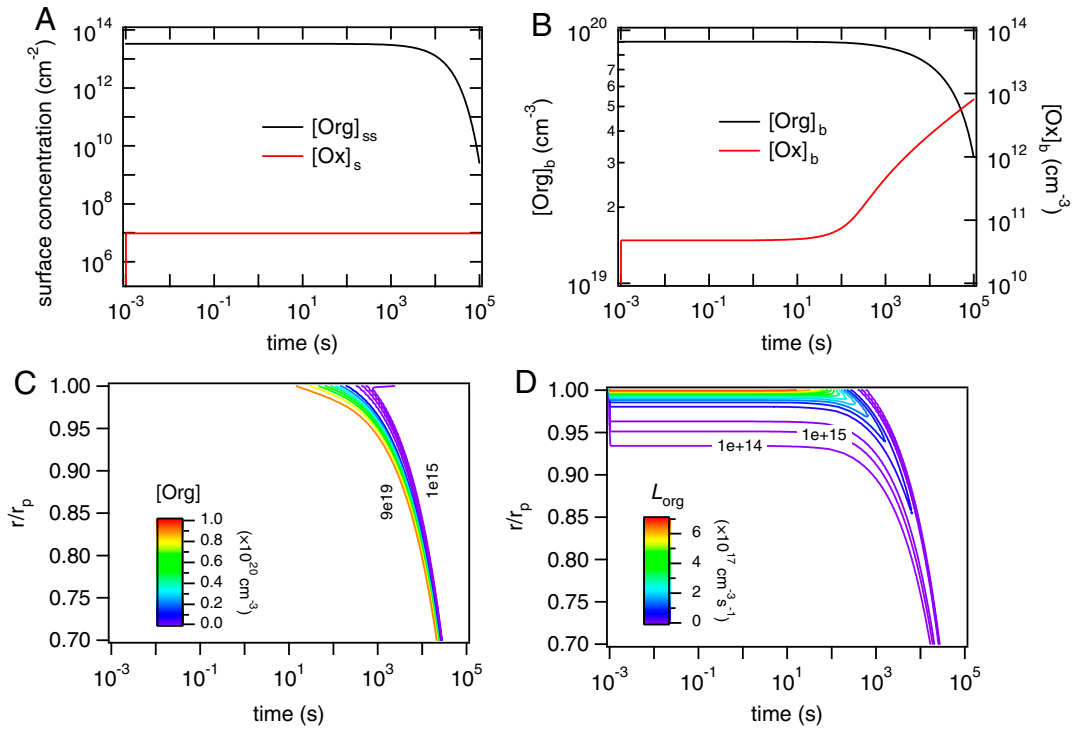

Fig. S2. Kinetic model results for the ozone uptake by semisolid protein (BSA) at 42 ppb O_3 and 50% RH at 296 K calculated with KM-SUB using input parameters from Table S1. (*A*) Surface concentrations and (*B*) average bulk concentrations of ozone ([Ox], red line) and reactive amino acids ([Org], black line). (*C*) Radial profile of reactive amino acid bulk concentration ([Org]); r/r_p is the distance from the particle center normalized by the particle radius ($r/r_p = 1$ at the surface). (*D*) Loss rate profile of reactive amino acids (L_{org}), showing that the reaction front (region of maximum loss rate) progresses from $r/r_p = 0.99$ up to ~10 s to $r/r_p = 0.80$ after ~10^4 s.

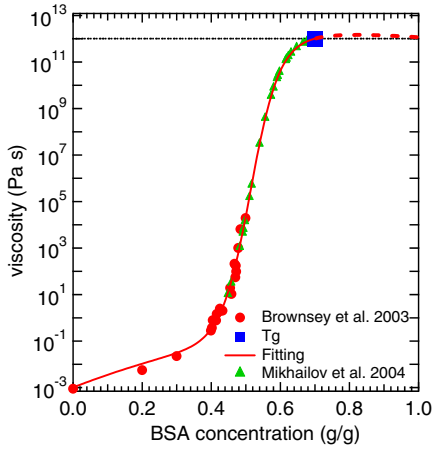

Fig. S3. Viscosity of aqueous BSA as a function of BSA mass fraction at 298 K. Experimental data from Brownsey et al. (1) (red circles) and at T_g of aqueous BSA at room temperature (blue square) were fitted using Eq. **S1** (red line). The green data points indicate the range of concentration and viscosity of aqueous BSA aerosol particles in the HTDMA experiments by Mikhailov et al. (2).

1 Brownsey GJ, Noel TR, Parker R, Ring SG (2003) The glass-transition behavior of the globular protein bovine serum albumin. *Biophys J* 85:3943–3950.

2 Mikhailov E, Vlasenko S, Niessner R, Pöschl U (2004) Interaction of aerosol particles composed of protein and salts with water vapor: hygroscopic growth and microstructural rearrangement. *Atmos Chem Phys* 4:323–350.

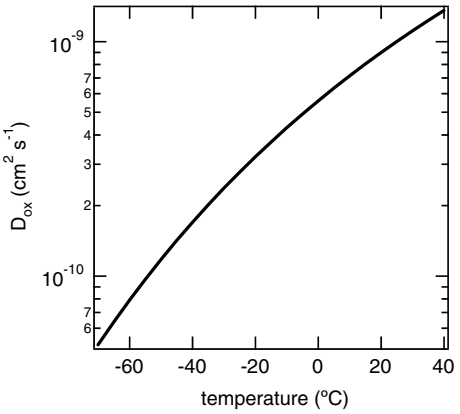

Fig. S4. Diffusion coefficient of ozone in aqueous BSA at 50% RH calculated as a function of temperature.

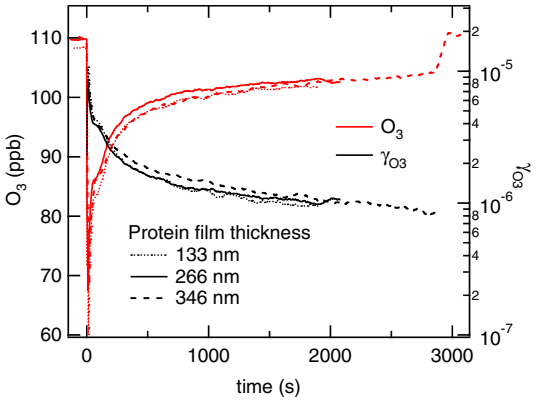

Fig. S5. Measurement data of ozone uptake experiments with protein films (BSA) at 50% RH. The uptake coefficient (γ_{O_3}) did not change when the protein film thickness was increased from 133 nm to 346 nm, indicating that the ozone uptake was kinetically limited by processes at or near the surface of the protein film.

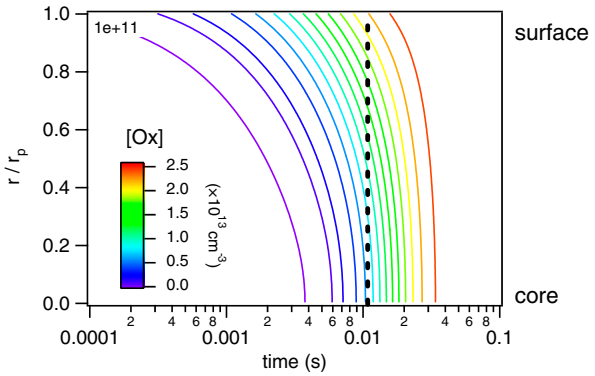

Fig. S6. Radial profile of ozone bulk concentration ([Ox]) for nonreactive uptake into a particle with 200 nm diameter and $D_{ox} = 10^{-9}$ cm^2 s^{-1} at 42 ppb O_3 and 50% RH calculated with KM-SUB using input parameters from Table S1; r/r_p is the distance from the particle center normalized by the particle radius ($r/r_p = 1$ at the surface). After the characteristic time of diffusion, $\tau_{cd} \approx 0.01$ s (black dotted line), the concentration at the particle core ($\approx 8 \times 10^{12}$ cm^{-3}) reaches $\sim 1/e$ of that in the near-surface bulk ($\approx 2.4 \times 10^{13}$ cm^{-3}).

Table S1. Kinetic parameters for the interaction of ozone and reactive amino acids in amorphous protein at 50% RH and 296 K

Parameter (Unit)	Value	Reference
$\alpha_{s,0}$	1	(1)
τ_d (s)	10^{-9}	(1)
k_{SLR} ($cm^2\ s^{-1}$)	10^{-11}	(2)
k_{BR} ($cm^3\ s^{-1}$)	1.6×10^{-15}	(3)
$K_{sol,cc}$ ($mol\ cm^{-3}\ atm^{-1}$)	10^{-3}	(4)
D_{ox} ($cm^2\ s^{-1}$)	10^{-9}	*SI Text*
D_{org} ($cm^2\ s^{-1}$)	10^{-20}	*SI Text*

*$\alpha_{s,0}$: surface accommodation coefficient of ozone on adsorbate-free substrate, τ_d: desorption lifetime of ozone, k_{SLR}: second-order rate coefficients of surface reaction between ozone and reactive amino acids, k_{BR}: second-order rate coefficients of bulk reaction between ozone and reactive amino acids, $K_{sol,cc}$: Henry's law coefficient of ozone, D_{ox} and D_{org}: bulk diffusion coefficients of ozone and reactive amino acids.

1 Shiraiwa M, et al (2011) The role of long-lived reactive oxygen intermediates in the reaction of ozone with aerosol particles. *Nature Chemistry* 3:291–295.
2 Pfrang C, Shiraiwa M, Pöschl U (2010) Coupling aerosol surface and bulk chemistry with a kinetic double-layer model (K2-SUB): an exemplary study of the oxidation of oleic acid by ozone. *Atmos Chem Phys* 10:4357–4557.
3 Sharma VK, Graham NJD (2010) Oxidation of amino acids, peptides, and proteins by ozone: a review. *Ozone Sci Eng* 32:81–90.
4 Ammann M, Pöschl U (2007) Kinetic model framework for aerosol and cloud surface chemistry and gas-particle interactions—Part 2: exemplary practical applications and numerical simulations. *Atmos Chem Phys* 7:6025–6045.